# Statistical analysis of solar activity variations of total electron content derived at Jet Propulsion Laboratory from GPS observations

Libo Liu[1] and Yiding Chen[1]

[1]   We analyzed the data series of the total electron content (TEC) derived at Jet Propulsion Laboratory from Global Positioning System (GPS) observations to investigate the solar activity effects of TEC on a global scale. The daily values of the solar extreme ultraviolet (EUV) fluxes in 0.1–50 nm wavelengths, 10.7 cm radio flux $F_{10.7}$, and $F_{10.7P}$ (the average of daily $F_{10.7}$ and its 81-day mean $F_{10.7A}$) are adopted to represent the solar EUV variability, respectively. The EUV fluxes are measured by the Solar EUV Monitor (SEM) spectrometer aboard Solar Heliospheric Observatory (SOHO). Three kinds of patterns (linearity, saturation, and amplification) can be detected in TEC versus $F_{10.7P}$ and EUV. A saturation feature exists in TEC versus $F_{10.7}$ in the daytime, more pronounced at low latitudes than at middle and high latitudes. The saturation in the equatorial anomaly regions is strongest in equinoxes and weakest in the June solstice. In contrast, the amplification in TEC, as a novel feature, is mainly distributed in the northern middle, and high latitudes in the December solstice and in the Southern Hemisphere in the June solstice and the March equinox. It is the first time to determine where and when the linear, saturation, and amplification patterns are distributed in TEC. Further, the solar activity sensitivity of TEC is stronger at day than at night and more evident at lower latitudes than at higher latitudes. The solar activity dependent rates of TEC in the equatorial and low-latitude regions have a minimum around the dip equator and maxima on both sides of the dip equator (near the crest of the equatorial anomaly). This structure is roughly aligned along the dip equator, being strongest in equinoxes and weakest in the June solstice, which highlights the importance of ionospheric dynamics related with $\mathbf{E} \times \mathbf{B}$ drift. In addition, this analysis confirms that in a statistical sense, a quadrate polynomial can well capture the long-term solar activity dependency of TEC at specified local time.

## 1.   Introduction

[2]   It is well known that solar radiation provides the primary energy source for upper atmospheric dynamics, energetics, and ionization. The magnitude of solar radiation varies with various timescales, which will significantly modulate the upper atmospheric structure, climate, and weather, inducing remarkable changes in the system of the terrestrial thermosphere and ionosphere [e.g., *Gorney*, 1990; *Hedin*, 1984]. Our interest here is on the ionospheric responses to the regular solar activity variations in solar extreme ultraviolet (EUV) and X-ray radiations. Indeed, as primarily ionizations for the ionosphere, solar EUV, and X-ray radiation can vary by more than a factor of 2 from solar minimum to solar maximum and by as much as 50% during a solar rotation [see *Lean et al.*, 2001; *Tobiska et al.*, 2000]. Thus the regular variations in solar EUV and X-ray radiations will strongly affect the Earth's ionosphere [*Afraimovich et al.*, 2008; *Balan et al.*, 1993, 1994; *Chakraborty and Hajra*, 2008; *Chen et al.*, 2008; *Huang*, 1967; *Huang and Cheng*, 1995; *Kane*, 1992, 2003; *Kouris et al.*, 1998; *Liu et al.*, 2003, 2004a, 2006; *Min et al.*, 2009; *Rich et al.*, 2003; *Richards*, 2001; *Rishbeth*, 1993; *Sethi et al.*, 2002; *Su et al.*, 1999] and the thermosphere [e.g., *Guo et al.*, 2007; *Hedin*, 1984; *Liu et al.*, 2005, 2004b], producing prominent solar activity effects of the ionosphere and thermosphere. As a result, the most prolonged solar activity effects should be taken into account in ionospheric models constructed for single stations, regions, and global as well to reproduce the dominant patterns of ionospheric parameters [e.g., *Belehaki et al.*, 2001; *Bilitza*, 2000; *Holt et al.*, 2002; *Liu et al.*, 2004a; *Pancheva and Mukhtarov*, 1998; *Zhao et al.*, 2005]. Among these models, the International Reference Ionosphere (IRI) model [see *Bilitza*, 2001] is the one most widely used. Further, the solar cycle effects on the ionosphere and thermosphere should be considered essentially in questions of space weather, climatology, and

---

[1]Beijing National Observatory of Space Environment, Institute of Geology and Geophysics, Chinese Academy of Sciences, Beijing, China.

long-term trends [e.g., *Laštovička*, 2009] of the ionosphere and thermosphere as well.

[3] In the past decades, many investigations have been conducted to explore the solar activity effects of several ionospheric parameters, such as electron density $N_e$ and plasma temperatures at different altitudes, total electron content (TEC), and peak electron density ($N_mF_2$) and peak height ($h_mF_2$) of the $F_2$ layer, in terms of observations and theoretical models as well [e.g., *Kane*, 2003; *Lei et al.*, 2005; *Liu et al.*, 2007a, 2007b; *Pandey et al.*, 2003; *Richards*, 2001; *Su et al.*, 1999]. Considerable progress has been achieved in the solar cycle variations of the ionosphere [*Sojka et al.*, 2006]. These investigations illustrate prominent and complicated solar cycle variations in the ionosphere. The relationship between $f_oF_2$ (or $N_mF_2$, TEC, etc.) and solar indices (sunspot number, solar 10.7 cm radio flux $F_{10.7}$, etc.) or solar EUV fluxes has been found to be roughly linear [e.g., *Balan et al.*, 1993, 1994; *Chakraborty and Hajra*, 2008; *Gorney*, 1990; *Kane*, 1992; *Kouris et al.*, 1998; *Lei et al.*, 2005; *Rishbeth*, 1993], two-segmented linear pattern [e.g., *Balan et al.*, 1994; *Bilitza*, 2000; *Liu et al.*, 2003], quadratic or higher polynomial functions [*Belehaki et al.*, 2001; *Chen et al.*, 2008; *Gupta and Singh*, 2001; *Huang*, 1967; *Kouris et al.*, 1998; *Liu et al.*, 2004a, 2006, 2007b; *Pancheva and Mukhtarov*, 1998; *Richards*, 2001; *Sethi et al.*, 2002], and even more complicated patterns [*Su et al.*, 1999; *Huang and Cheng*, 1995]. Further, several investigations reported a hysteresis feature (i.e., the nonlinear dependency on the states of the historical solar cycle phase) [e.g., *Burešová and Laštovička*, 2000; *Chakraborty and Hajra*, 2008; *Mikhailov and Mikhailov*, 1995; *Rao and Rao*, 1969; *Trísková and Chum*, 1996], which is small at low and high latitudes but substantial at midlatitudes [*Kane*, 1992].

[4] In fact, many works suffered from poor spatial and/or temporal coverage, due to limited spatial coverage of ionosonde data and/or time duration of TEC data, so complete global-scale patterns on the solar cycle variations of the ionosphere have not been clearly reported. Up to now, we do not know the detailed features of the solar activity effects of the ionosphere and the related processes fully at all.

[5] It is essential that long-time records of both the ionosphere and solar EUV and X-ray radiation data set are available to track more accurately the solar activity effects on the ionosphere [*Bilitza*, 2000]. The solar EUV and X-ray emission is totally absorbed in the upper atmosphere and cannot approach the surface of the Earth; thus the observations of solar EUV cannot be directly made on the ground and more than 2 decades space-based measurements of solar EUV are unfortunately intermittent. In the absence of continuous long-term records of EUV data, most researches had to rely on ground-based solar indices, such as sunspot number and $F_{10.7}$, although it has long been realized that neither sunspot number nor $F_{10.7}$ is ideal for representing solar EUV variability [*Lean et al.*, 2001].

[6] Since 1996, solar EUV fluxes in $26-34$ nm and $0.1-50$ nm wavelength ranges were continuously monitored by the Solar EUV Monitor (SEM) spectrometer aboard the Solar Heliospheric Observatory (SOHO) [*Judge et al.*, 1998], which offer us the longest solar EUV data set. Utilizing the SOHO/SEM EUV records, *Liu et al.* [2006]

confirmed that in statistical sense $F_{10.7P}$ represents fairly well the intensity of solar EUV fluxes [*Hinteregger et al.*, 1981; *Richards et al.*, 1994]. $F_{10.7P} = (F_{10.7} + F_{10.7A})/2$, and $F_{10.7A}$ is the 81 days mean of daily $F_{10.7}$. Therefore $F_{10.7P}$ is recommended to be a new solar proxy for common use, which has the advantages of long-term records and easy availability as $F_{10.7}$ does.

[7] With the advent of Global Positioning System (GPS), dual-frequency GPS receivers are routinely operated with global coverage. It provides us an excellent data source to explore the global-scale ionosphere in unprecedented details. Information on TEC can be derived from these GPS observations, and global ionospheric maps (GIM) of TEC are routinely produced at five analysis centers [e.g., *Mannucci et al.*, 1998].

[8] We utilize the SOHO/SEM EUV data and the TEC GIMs produced at Jet Propulsion Laboratory (JPL) to quantify the global-scale response of the ionosphere to solar EUV forcings. This analysis elucidates some detailed features of the solar activity effects on TEC, including seasonal and local time variations and longitudinal and latitudinal dependencies as well. Our results support that in a statistical sense, a quadratic regression can fit the solar activity dependency of TEC fairly good for prediction purpose [*Huang*, 1967]. We reveal that there are three types of patterns in the solar activity effects of TEC, that is, linear, saturation, and amplification, respectively. The most interesting finding is that the patterns of the solar activity sensitivity of TEC present a marked latitudinal structure, which varies with season and local time. The detailed latitudinal range of the saturation and amplification features of global-scale TEC on solar activity is reported for the first time.

## 2. GPS TEC and Solar EUV Data

[9] TEC GIMs are routinely produced at five analysis centers on the basis of measurements of GPS receivers from the international network and other institutions [e.g., *Iijima et al.*, 1999; *Mannucci et al.*, 1998]. We used the vertical TEC generated at JPL. The TEC is modeled in a solar-geomagnetic reference frame using bicubic splines on a spherical grid. A Kalman filter is applied to solve simultaneously for TEC and instrumental biases. Each TEC map in the solar-geomagnetic reference frame is then transformed into an Earth-fixed reference frame on global grids with geographic longitude ranging from $-180°$ to $180°$ (with a $5°$ resolution) and latitude from $-87.5°$ to $87.5°$ ($2.5°$ resolution), which are available from the JPL website in the form of Ionosphere Map Exchange format (IONEX) files with a temporal resolution of 2 h. The reader is referred to *Mannucci et al.* [1998] for a detailed description of the deviation procedure of TEC from measurements of global GPS receivers.

[10] Meanwhile, we use the daily values of $F_{10.7}$ and SOHO/SEM EUV fluxes (in $0.1-50$ nm wavelength ranges) to indicate the solar EUV variability. *Liu et al.* [2006] illustrated a perfect correlation between the SOHO/SEM EUV fluxes in $26-34$ nm and $0.1-50$ nm wavelength ranges [*Judge et al.*, 1998]. A nonlinear relationship is found in $F_{10.7}$ versus several solar data and proxies (Lyman $\alpha$, He I 1083, and Mg II). In contrast, $F_{10.7P}$ can represent

linearly the intensities of SEM/SOHO EUV and other solar proxies with improved correlations. Therefore we collected the JPL TEC data in IONEX files from September 1998 to April 2009 as well as the corresponding EUV fluxes (0.1–50 nm), $F_{10.7}$ and $F_{10.7P}$ to investigate the solar activity effects of TEC on global scale. Values of TEC on each day at specified local times are obtained through a linear interpolation from the TEC data series. In the following sections we choose data in about 2 months, i.e., day of year (DOY) during [60, 120], [160, 220], [250, 310], and [335, 30], to analyze the behaviors of TEC in the March equinox, June solstice, September equinox, and December solstice, respectively.

## 3. Results

### 3.1. TEC Versus Solar EUV, $F_{10.7}$, and $F_{10.7P}$

[11] Figure 1 shows the mass plots of TEC (in units of $10^{16}$ electrons/m$^2$, denoted by TECu) on individual days at 1400 LT (local time) over seven geographic latitudes along longitude 120°E against SEM/SOHO EUV (0.1–50 nm) (in unit of $10^9$ photons·cm$^{-2}$·s$^{-1}$), $F_{10.7}$ (in solar flux unit, 1 sfu = $10^{-22}$ W·m$^{-2}$·Hz$^{-1}$) and $F_{10.7P}$ during DOY [250, 310]. For simplicity, we denote EUV (0.1–50 nm), $F_{10.7}$, and $F_{10.7P}$ as $S$, $F$, and $P$, respectively. In Figure 1 we only show the quadratic fitting results (see the equations and the solid curves in Figure 1). In fact, we have applied a piecewise linear fitting as well as polynomial fittings of TEC versus $S$, $F$, and $P$. The analyses show that the piecewise linear fitting agrees well with the quadratic results; that is, in statistical sense, a quadratic regression:

$$TEC(I) = A_0 + A_1 I + A_2 I^2 \qquad (1)$$

can describe the solar activity dependency of TEC fairly good for practice purposes. Here $A_0$, $A_1$, and $A_2$ are the coefficients, and $I$ in equation (1) denotes $F$, $P$, and $S$, respectively. In Figures 1, 3, and 5, $A_1(TEC, F)$ and $A_1(TEC, P)$ are in units of TECu/sfu, $A_1(TEC, S)$ in $10^{-9}$ TECu/photons·cm$^{-2}$·s$^{-1}$, respectively. In Figure 1, $A_2(TEC, F)$ and $A_2(TEC, P)$ are in units of TECu/sfu$^2$, and $A_2(TEC, S)$ in $10^{-18}$ TECu/photons$^2$·cm$^{-4}$·s$^{-2}$; while in Figures 3 and 5, $A_2(TEC, F)$ and $A_2(TEC, P)$ are in units of $10^{-3}$ TECu/sfu$^2$, and $A_2(TEC, S)$ in $10^{-21}$ TECu/photons$^2$·cm$^{-4}$·s$^{-2}$. The sign of $A_2$ indicates the possible nonlinear trend, being an amplification trend for a positive $A_2$, a saturation trend for a negative $A_2$, and a linear one for an ignoring $A_2$; while the ratio of the linear term and the third term determines the nonlinear extent, being more linear with a higher value of this ratio. We identified that for application purposes, a quadratic regression is an optimum choice, and higher-order regressions cannot significantly improve the fitting anymore. Similar quadratic regressions have been used in the work of *Gupta and Singh* [2001], *Huang* [1967], *Kouris et al.* [1998], *Liu et al.* [2004a], *Sethi et al.* [2002], and so on. The same conclusion can also be drawn from the monthly median data, although we only showed the analyses of the daily data here. We recommend the community that a quadratic regression should be used to optimally describe the solar activity effects of TEC in theoretical analyses and empirical ionospheric models. For

example, the two-segmented linear pattern in IRI [e.g., *Bilitza*, 2000] can be replaced with equation (1).

[12] As illustrated in Figure 1, strong solar activity effects can be detected in TEC versus $S$, $F$, and $P$, with an apparent latitudinal dependence. There are somewhat differences between TEC versus $F$, $P$, and $S$. The values of TEC on individual days are apparently nonlinear with those of $F$. That is, there are significant saturation features in TEC versus $F$ at most latitudes, being stronger at low latitudes. A similar feature has been reported in TEC [e.g., *Balan et al.*, 1994], $f_oF_2$ [*Kane*, 1992; *Liu et al.*, 2003], and in $N_mF_2$ [*Chen et al.*, 2008; *Liu et al.*, 2004a, 2006; *Richards*, 2001], respectively.

[13] In contrast, at many latitudes there is roughly a linear pattern in TEC versus $S$ and $P$, and the scatter also becomes smaller in the latter two results. The behaviors are found to be identical in TEC versus $S$ and $P$. The saturation feature in TEC versus $S$ and $P$ becomes quite weaker in many regions, but it can still be detected at some latitudes (e.g., TEC at 10°N and 10°S versus $P$). This coincides with that of $N_mF_2$ or $f_oF_2$ [*Liu et al.*, 2003, 2006] and shows some discrepancies from *Balan et al.* [1993, 1994]. Of course, the saturation behavior is more evident in $N_mF_2$ than in TEC. Moreover, as indicated by the sign of $A_2$ of these fitting equations in Figure 1, an amplification feature can be seen in TEC versus $S$ and $P$ at some locations (e.g., TEC at 50°N). It is interesting that the amplification is a novel feature in TEC, although the amplification feature has been reported in the nighttime $f_oF_2$ [e.g., *Chen et al.*, 2008; *Liu et al.*, 2004a], topside plasma density [*Chen et al.*, 2009; *Liu et al.*, 2007b], and the mean TEC, being stronger amplification feature at higher latitudes [*Liu et al.*, 2009].

[14] We calculated the linear correlation coefficients r(TEC, F), r(TEC, P), and r(TEC, S) between TEC along longitude 120°E versus $S$, $F$, and $P$, respectively, as a function of local time and geographic latitude in four seasons. The linear correlation coefficients r(TEC, F), r(TEC, P), and r(TEC, S) between TEC versus $S$, $F$, and $P$ are generally quite high, ~0.9 in the daytime. The correlations decrease somewhat in the nighttime, especially in the early morning at some locations.

### 3.2. Solar Activity Effects of TEC Along Longitude 120°E

[15] Equation (1) can well capture the solar activity dependences of TEC in statistical sense, as shown in section 3.1. Thus coefficients $A_1$ and $A_2$ in equation (1) should reflect the solar activity sensitivity of TEC. Contours of coefficients $A_1$ and $A_2$ in quadratic fittings of TEC along longitude 120°E versus $F$ (left), $P$ (middle), and $S$ (right) with local time and geographic latitude in four seasons are plotted in Figure 2 and Figure 3, respectively. The solid white line denotes the geographic latitude of the dip equator at longitude 120°E.

[16] Contours of $A_1$ in Figure 2 reveal apparent local time and seasonal variations and latitude dependences in the solar activity sensitivity of TEC. A strong day-night difference can be detected in $A_1$, with high values at day and low ones at night. The diurnal $A_1$ increases after sunrise and reaches its peak at around 1400 LT. It then decreases and minimizes in the presunrise hours. The values of $A_1$ are the highest in equinoxes (DOY in [60, 120] and [250, 310]).
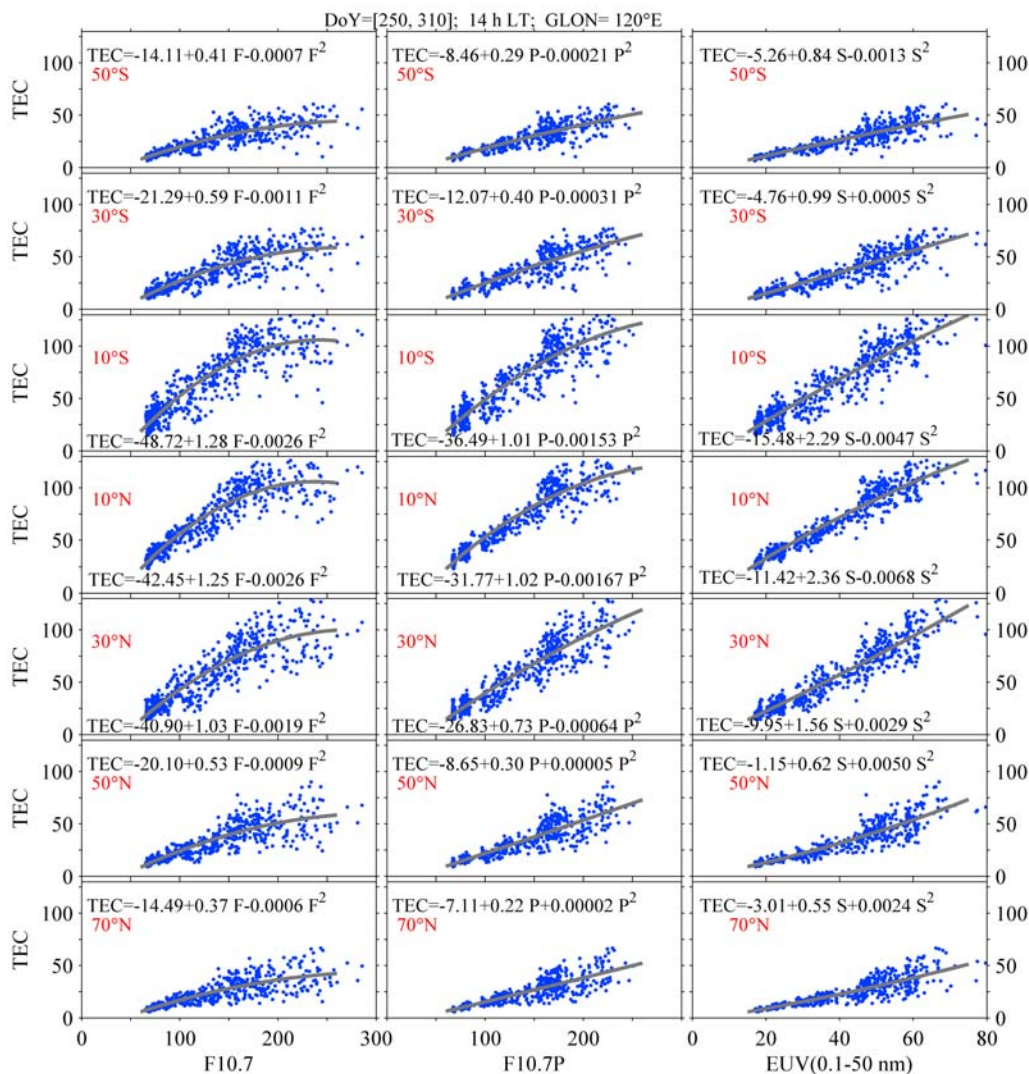
**Figure 1.** Mass plots of daily Jet Propulsion Laboratory (JPL) GPS total electron content (TEC) (in units of $10^{16}$ electrons/m$^2$, denoted by TECu) at 1400 LT over seven geographic latitudes along longitude 120°E versus $F_{10.7}$ (in solar flux unit, 1 sfu = $10^{-22}$ W·m$^{-2}$·Hz$^{-1}$), $F_{10.7P}$ (=($F_{10.7}$ + $F_{10.7A}$)/2, $F_{10.7A}$ is the 81-day mean value of daily $F_{10.7}$ centered on the specific day), and the daily average Solar Heliospheric Observatory (SOHO)/Solar Extreme Ultraviolet (EUV) Monitor (SEM) full solar disk EUV flux in 0.1–50 nm wavelength interval (in unit of $10^9$ photons·cm$^{-2}$·s$^{-1}$) at 1 AU during day of year (DOY) [250, 310] in the years from 1998 to April 2009. The curves and equations denote a quadratic polynomial fitting of the data. Here F stands for $F_{10.7}$, P stands for $F_{10.7P}$, and S stands for SOHO/SEM EUV flux (0.1–50 nm).

It is important to note that in equinoxes the latitudinal variation of $A_1$ in daytime is basically symmetric about the dip equator, denoting by the white line in Figure 2, while it becomes asymmetric in solstices (DOY in [160, 220] and [335, 30]), with higher $A_1$ in the winter hemisphere. Moreover, the values of $A_1$ are higher at low latitudes than at higher latitudes. A pronounced feature is that the daytime $A_1$ is found to maximize in the vicinity of the crests of the equatorial ionization anomaly (EIA) and minimize near the dip equator. This latitudinal structure appears at around 1000 LT and persists till late evening. Similar latitudinal feature has also been found in the solar activity effects of $N_mF_2$ during daytime [*Liu et al.*, 2006] and near 2100 LT [*Whalen*, 2004] and also in the thermo-spheric total mass density derived from CHAMP [*Liu et al.*, 2005]. This EIA-like structure in $A_1$ is more distinct, develops earlier, and lasts longer in equinoxes than in solstices. During solstices, the $A_1$ crest in the winter hemisphere is stronger and is located closer to the dip equator, compared to the summer one.

[17] Further, contours of $A_2$ in Figure 3 illustrate the nonlinear characteristic of the dependence of TEC on $F$, $P$, and $S$. It is clearly seen that the nonlinear extent of the dependency of TEC on solar activity levels are distinct with latitudinal and local time differences. The most important point is that there are three kinds of patterns in the solar activity dependences of TEC, that is, linear, saturation, and amplification, respectively. It is the first time to report the
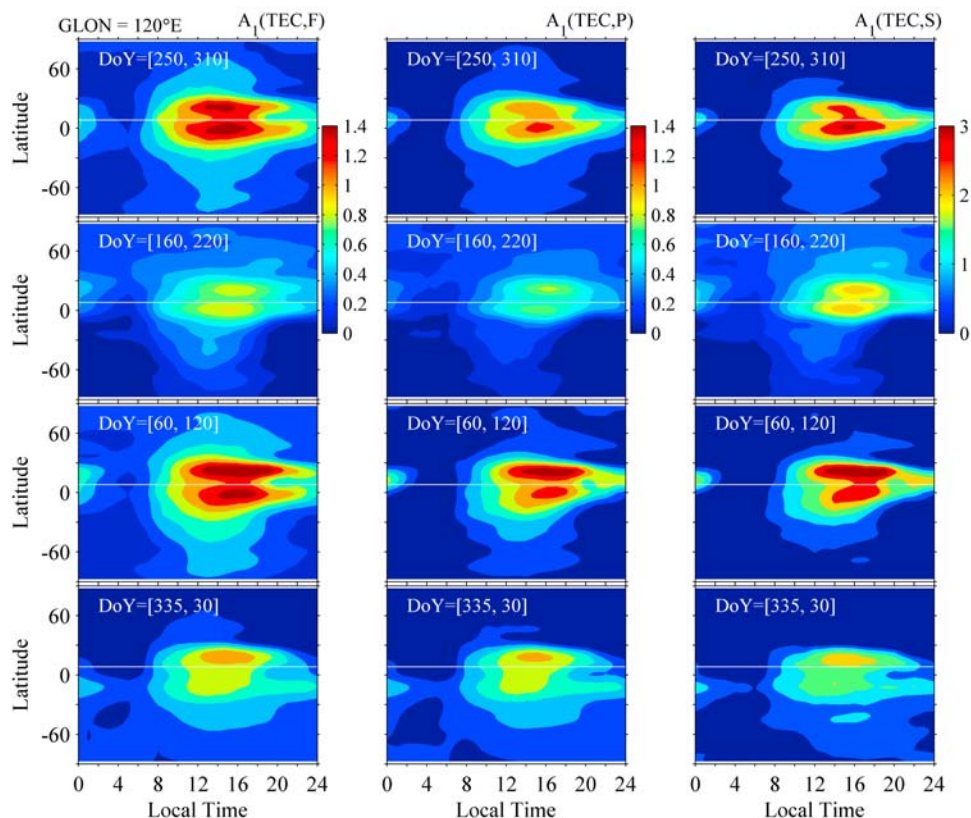
**Figure 2.** Contours of the coefficient $A_1$ in a quadratic fitting of TEC versus (left) F, (middle) P, and (right) S with local time and geographic latitude for four seasons along longitude 120°E. Here $A_1$(TEC, F) and $A_1$(TEC, P) in units of TECu/sfu, and $A_1$(TEC, S) in $10^{-9}$ TECu/photons·cm$^{-2}$·s$^{-1}$, respectively. The solid white line denotes the geographic latitude of the dip equator at longitude 120°E.

amplification pattern in the solar activity dependences of TEC. Another distinct feature is that there is an EIA-like structure in the latitudinal variation of $A_2$ in the daytime, with higher negative values on both sides of the dip equator. It is also the first time to show the latitude range where the saturation effect of TEC is present. *Liu et al.* [2003] and *Liu et al.* [2006] revealed significant saturation effects in $f_oF_2$ or $N_mF_2$ in the EIA region; however, the poor spatial resolution of the ionosonde stations hinders them to determine the latitude range of the saturation effect. The double crests of negative $A_2$(TEC, P) (see Figure 3) are reasonable consistent with the significant saturation feature of $N_mF_2$ in the EIA region, which further support the argument that ionospheric dynamical processes are important for the saturation effect [*Liu et al.*, 2003, 2006]. The distributions of the sign of $A_2$(TEC, P) are generally rather similar to those of $A_2$(TEC, S) in all seasons and are somewhat different from those of $A_2$(TEC, F). A key difference is that, the amplification pattern can be found somewhere in $A_2$(TEC, P) and $A_2$(TEC, S) in four seasons, while this pattern is absent in $A_2$(TEC, F).

[18] Figure 4 depicts the local time and seasonal variations of $A_1$(TEC, P) at five latitudes ranging from equatorial to middle latitudes along longitude 120°E. As Figure 4 indicated, $A_1$(TEC, P) varies diurnally with a minimum in the morning before sunrise and a flat peak in the time interval from local noon to 1800 LT, which is dependent on latitude and season (or DOY). The seasonal variation of $A_1$

has latitudinal differences. The daytime $A_1$(TEC, P) in the dip equatorial and low-latitude regions (the cases at latitude 25°N, 10°N, and 5°N) shows two peaks around equinoxes and is higher in the December solstice than in the June solstice. $A_1$ at higher latitudes (e.g., the cases at latitude 45°N and 45°S) is found to maximize in local summer and minimize in local winter months. Moreover, the day-to-night difference of $A_1$ is more distinct in equatorial and low-latitude regions than at higher latitudes.

### 3.3. Solar Activity Effects of TEC on Global Scale

[19] Figure 5 shows the global distributions of $A_1$(TEC, P) and $A_2$(TEC, P) at 1400 LT in four seasons.

[20] The values of $A_1$(TEC, P) reach peaks in equatorial and low latitude regions. In most longitude sectors there is a remarkable double-peak structure in $A_1$ in the EIA region with a minimum at around the dip equator and maxima on both sides of it. This latitudinal structure of $A_1$ is quite similar to the EIA in the equatorial ionospheric $F_2$ layer. *Whalen* [2004] also reported such a crest structure in the solar dependent rate of $N_mF_2$ in the Northern Hemisphere. In the longitude ranges around longitude 0° the double peaks virtually disappear and they are merged into a single peak in most seasons. Outside the EIA region, the values of $A_1$(TEC, P) decrease with latitude, which agrees with that reported by *Huang and Cheng* [1995]. It deserves to note that, unfortunately, the conclusions of *Huang and Cheng*
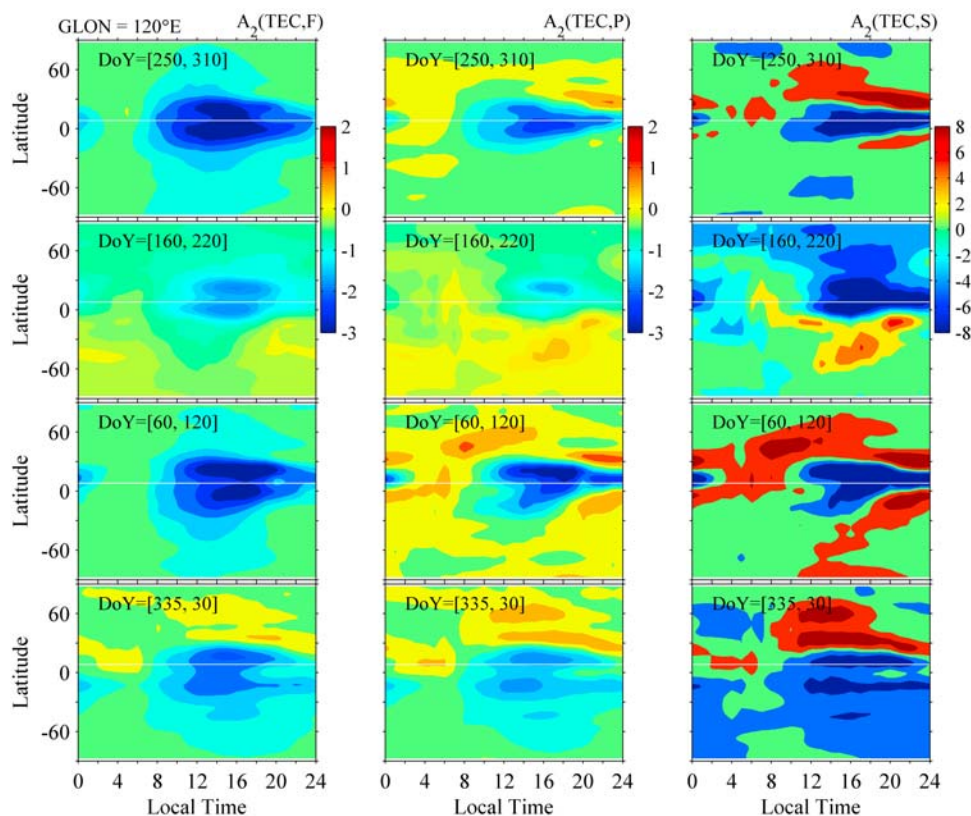
**Figure 3.** Contours of the coefficient $A_2$ in the quadratic fitting of TEC versus (left) F, (middle) P, and (right) S with local time and geographic latitude for four seasons along longitude 120°E. Here $A_2$(TEC, F) and $A_2$(TEC, P) in units of $10^{-3}$ TECu/sfu$^2$, and $A_2$(TEC, S) in $10^{-21}$ TECu/photons$^2$·cm$^{-4}$·s$^{-2}$, respectively. The solid white line denotes the geographic latitude of the dip equator at longitude 120°E.

[1995] were based on the TEC measurements only at three locations.

[21] There is an indication that the changes of TEC have substantial contributions from different factors. The global distribution of $A_1$ illustrates the control effects of ionospheric dynamics and the geomagnetic configuration on the solar activity sensitivity of TEC. The equatorial minimum of $A_1$ is roughly aligned along the dip equator, which reflects the effects of the geomagnetic configuration or the dominant role of $\mathbf{E} \times \mathbf{B}$ drift in the equatorial region. Moreover, double peaks of $A_1$ in Figures 2 and 5 at equatorial and low latitudes provide convincing evidence of the important role of ionospheric dynamics, and the latitudinal asymmetry in $A_1$ highlights the effects of neutral winds and the neutral compositions as well. The F region plasma in the EIA region is dominantly controlled by the well-known "fountain effect." Hence $A_1$ in the EIA region will subject to significant dynamical influences as shown in Figures 2 and 5. *Whalen* [2004] had emphasized the role of $\mathbf{E} \times \mathbf{B}$ drift on the solar dependence of $N_mF_2$ in the EIA regions, especially around postsunset.

[22] Similar to the situation at longitude 120°E, there are apparent seasonal variations in global $A_1$(TEC, P). At equatorial and low latitudes the values of $A_1$ show a semiannual variation, being higher in equinoxes (highest in the March equinox) and lower in solstices (lowest in the June solstice). At the altitudes of the CHAMP satellite the rates of electron density with P are stronger in equinoxes (highest around the March equinox) than in solstices in the EIA crest regions [*Liu et al.*, 2007]. Consistent feature can also be found in $N_mF_2$ [*Whalen*, 2004] and TEC over low latitudes (e.g., at Ramey (17°N, 289°E) (see Figure 10 of *Balan et al.* [1994]), Calcutta (22.58°N, 88.38°E) [*Chakraborty and Hajra*, 2008], and Delhi (28.63°N, 77.22°E) [*Gupta and Singh*, 2001]).

[23] At higher latitudes $A_1$ is generally greatest in local summer, minimizes in local winter, and takes intermediate values in equinoxes. It is somewhat different from previous investigations on $N_mF_2$. *Rishbeth* [1993] has reported the summer-winter difference in the solar activity sensitivity of midlatitude $f_oF_2$ and found that the midlatitude $F_2$ layer is more solar-controlled in winter than in summer. The values of $dN_mF_2/dP$ at Millstone Hill (42.6°N, 288.5°E) are higher in winter than in summer [*Lei et al.*, 2005]. *Liu et al.* [2006] reported that the overall seasonal behavior of $dN_mF_2/dP$ at midlatitudes is also higher in winter and lower in months from June to August. Of course, $A_1$(TEC, P) may be different from dTEC/dP, especially when there is strong nonlinearity in the solar dependence of TEC. We have also applied a linear fitting to TEC and found that the winter-to-summer difference of dTEC/dP is similar to that in $A_1$(TEC, P). The above seasonal discrepancy in the solar sensitivity of TEC and $N_mF_2$ may reflect the differences of the contributed processes.
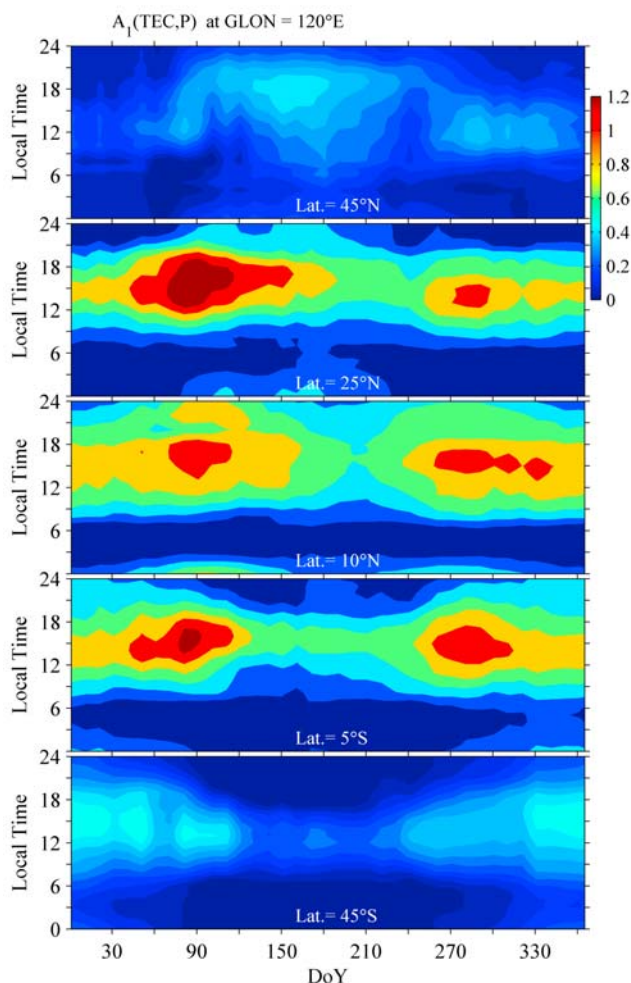
**Figure 4.** The seasonal and local time variations of $A_1(TEC, P)$ (in TECu/sfu) at five latitudes along longitude 120°E.

[24] In contrast, $A_2(TEC, P)$ shows a quite complicated structure. Two points can easily be detected. One is the saturation effect, which is indicated by the negative values of $A_2$ in the equatorial and low latitude regions. As shown in Figure 5, the minimum $A_2$ is also located roughly the same latitudes as the double peaks of $A_1$. Furthermore, the strength of the negative values of $A_2$ varies with season, being least in the June solstice and greater in other seasons. *Whalen* [2004] identified the essential role of $\mathbf{E} \times \mathbf{B}$ drift on the solar activity effects of $N_mF_2$ in the equatorial region. Our low latitude results also highlight the importance of ionospheric dynamics related with $\mathbf{E} \times \mathbf{B}$ drift. Another fascinating feature is the amplification effect as reflected by a positive $A_2$. As Figure 5 displays, the positive $A_2$ is mainly distributed in the Northern Hemisphere (middle and high latitudes) in the December solstice and in the Southern Hemisphere in the June solstice and the March equinox.

## 4. Discussions

[25] It is generally accepted that the most contribution to TEC comes from the electron density in the $F$ region [e.g.,

*Gupta and Singh*, 2001; *Richards et al.*, 1994]. Thus there is a close relationship of TEC with $N_mF_2$ and the behaviors of both parameters should generally share similar features. However, according to its definition, GPS TEC contains information of electron density along all the way of the integral from the receiver to the GPS satellites. It is also well known that the ionosphere has significant altitude dependence and the dominant processes at different altitudes are quite different. In the ionosphere at lower altitudes the photoionization and chemical processes are essential, while at high altitudes the dynamical processes gradually take over the control of the recombination and production processes.

[26] As a result, the solar activity effects of electron density in the ionosphere show interesting altitudinal dependence [e.g., *Su et al.*, 1999] and the behaviors of TEC and $N_mF_2$ may be different in some aspects. Linear and saturation effects are found in the solar activity dependency of daytime $N_mF_2$ or $f_oF_2$ [e.g., *Gorney*, 1990; *Huang*, 1967; *Kane*, 1992; *Kouris et al.*, 1998; *Lei et al.*, 2005; *Liu et al.*, 2004a, 2006; *Pancheva and Mukhtarov*, 1998; *Richards*, 2001; *Rishbeth*, 1993; *Sethi et al.*, 2002; *Whalen*, 2004; *Zhang and Holt*, 2007]. The amplification effect can be detected sometimes in nighttime $N_mF_2$ [e.g., *Chen et al.*, 2008; *Liu et al.*, 2004a]. In contrast, at high altitude (e.g., 800 km) the plasma density from DMSP show linear relationship with $F_{10.7}$ and amplify at growing rates with solar EUV [*Liu et al.*, 2007b]. This amplification prevails at 800 km altitude and is stronger in the equatorial region in the evening sector. Recently, *Chen et al.* [2009] found that at 600 km altitude this amplification pattern no more prevails. The patterns of linearity, saturation, and amplification all can be found in low latitudes at different local times; that is, the solar activity dependence of electron density at that altitude (600 km) varies with local time, season, and location.

[27] Turning to TEC, there are also complicated patterns as indicated by the results in section 3. The most fascinating feature is the amplification in TEC, which is reported for the first time. Past investigations [e.g., *Afraimovich et al.*, 2008; *Balan et al.*, 1993, 1994; *Chakraborty and Hajra*, 2008; *Huang and Cheng*, 1995; *Rastogi and Sharma*, 1971] mainly focused on the linearity and saturation. This amplification effect in TEC is a novel feature.

[28] We wish to mention a work recently be done by *Liu et al.* [2009], which is also based on the same TEC data source. They evaluated the mean TEC over specified latitude regions as well as globe and found that the saturation effect exists in those mean TEC versus $F_{10.7}$, more evident at lower latitudes; while an amplification effect can easily be detected in the mean TEC versus EUV, more marked at higher latitudes. It offers evidence that the amplification effect of TEC can exist over a wide range of locations, which can easily be identified by the distribution of positive $A_2$ in Figure 5 (right).

[29] Ion production in the ionosphere is proportional to the EUV flux, which can be related to the ambient electron density. However, ionization by direct solar flux is not the sole cause of electron density changes. Changes can also occur because of changes in neutral density, temperature and composition, the chemistry of the ionosphere, and neutral winds [e.g., *Liu et al.*, 2004b] and electric fields,
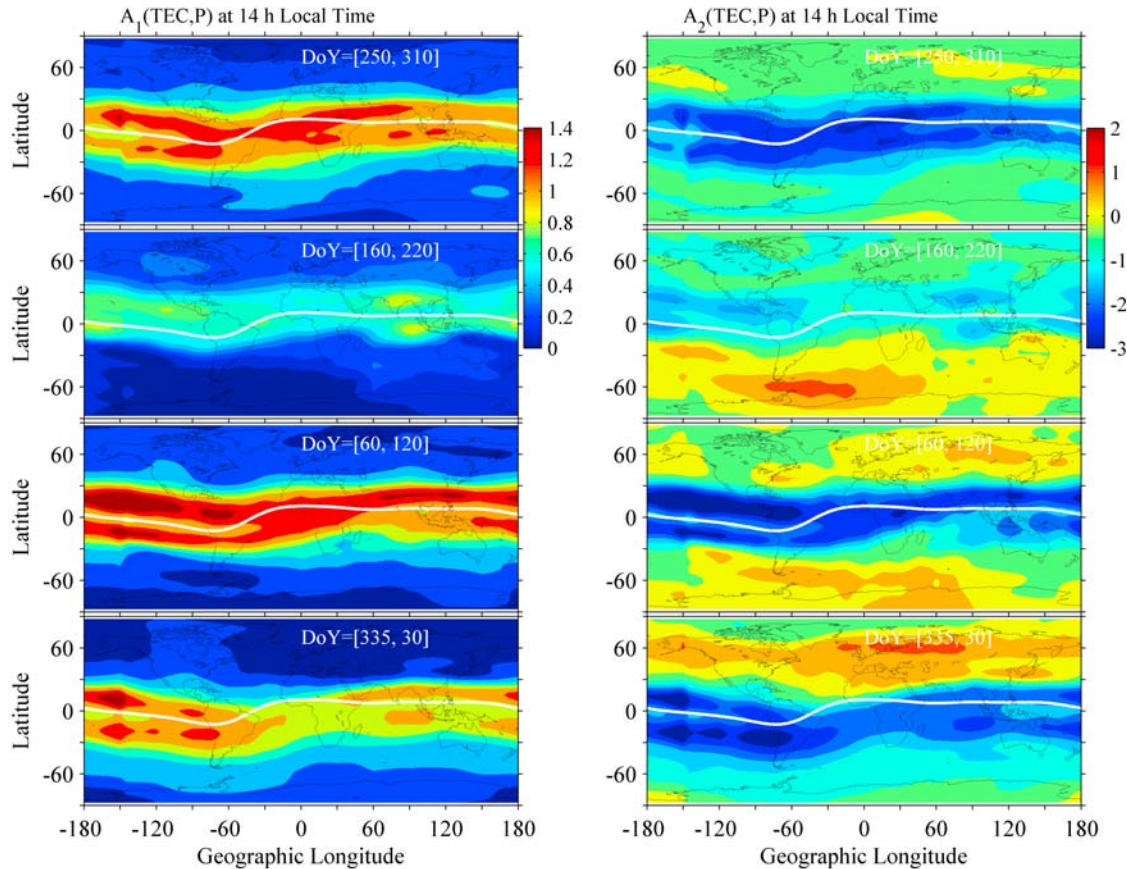
**Figure 5.** Global distribution of the coefficients $A_1$ and $A_2$ in the quadratic fitting of TEC versus P at 1400 LT for four seasons. $A_1(TEC, P)$ is in units of TECu/sfu, and $A_2(TEC, P)$ in units of $10^{-3}$ TECu/sfu$^2$. The solid curve denotes the location of the dip equator.

all of which vary with solar EUV and their relationship with electron density may not be linear [*Kane*, 2003].

[30] The complicated patterns existing in the solar activity effects of TEC can be qualitatively explained in terms of the discussions of *Chen et al.* [2008, 2009] and *Liu et al.* [2007b], if we realize the neutral compositions in the upper atmosphere, ionospheric scale heights and dynamical processes also vary with solar activity [e.g., *Hedin*, 1984; *Kutiev et al.*, 2006; *Liu et al.*, 2004b, 2007a]. We can qualitatively understand the amplification effect of TEC in the following way. To a first approximation, the electron density profile obeys a Champan-like function; thus TEC is related with the scale height $H$ and the peak electron density $N_mF_2$ in terms of

$$TEC = 2.82\, H \cdot N_mF_2. \qquad (2)$$

Here 2.82 in equation (2) is evaluated from Chapman-$\alpha$ profile; for other profiles, this number may be different. Then we have

$$\frac{d\,TEC}{dI} = 2.82\, H \cdot \frac{d\,N_mF_2}{dI} + 2.82\, N_mF_2 \cdot \frac{d\,H}{dI}. \qquad (3)$$

Equation (3) indicates that the solar activity variation of TEC is related with the solar activity variation of $N_mF_2$ and

that of $H$. If both $N_mF_2$ and $H$ present a linear solar activity dependency [e.g., *Liu et al.*, 2006, 2007a], we can expect a larger $\frac{d\,TEC}{dI}$ from higher values of $N_mF_2$ and $H$ at higher solar condition, according to equation (3). That possible larger $\frac{d\,TEC}{dI}$ at higher solar activity means an amplification feature in TEC. This is analog to the behavior of electron density in the topside ionosphere, e.g., at 800 km from DMSP observations [*Liu et al.*, 2007b]. When saturation occurs in $N_mF_2$, the solar activity behavior of TEC will be complicated. Of course, a quantitative evaluation [e.g., *Richards*, 2001] needs model simulations with the aid of long-term observations of neutral compositions and winds, electric fields, and so on. Unfortunately, these required observations are not available simultaneously at the current stage.

## 5.  Summary

[31] This study has analyzed the data of GIM TEC derived at JPL from September 1998 to April 2009 to investigate the solar activity features of TEC on global scale. In summary, the major results are outlined as follows.

[32] 1. There are remarkable differences between the dependences of TEC on $F_{10.7}$ and those of TEC on $F_{10.7P}$ and solar EUV. Three kinds of patterns (linearity, saturation, and amplification) can be detected in TEC versus $F_{10.7P}$ and solar EUV, while in TEC versus $F_{10.7}$ the saturation is

stronger by day and the amplification is not found. The amplification is a novel feature of the solar activity effects of TEC, which is not reported yet.

[33] 2. The TEC shows strong solar activity modulations with apparent seasonal and local time differences and latitudinal variations. It is the first time to determine when and where the saturation and amplification effects occur in TEC. The saturation effect exists in the daytime TEC in the equatorial and low latitudes, more evident at the EIA crest latitudes; while the amplification is mainly distributed in the northern middle and high latitudes in the December solstice and in the Southern Hemisphere in the June solstice and the March equinox. The global linear and quadratic coefficients in the equatorial and low-latitude regions are distributed aligning along the dip equator with a double peak structure, which suggests the effects of the geomagnetic configuration or the dominant role of $\mathbf{E} \times \mathbf{B}$ drift.

[34] 3. A quadratic regression can statistically describe the solar activity dependence of TEC for application purposes, and higher-order regressions do not significantly improve the fitting result anymore. Hence we recommend the community to apply a quadratic function in describing the solar activity effects of TEC in empirical models.

# References

Afraimovich, E. L., E. I. Astafyeva, A. V. Oinats, Y. V. Yasukevich, and I. V. Zhivetiev (2008), Global electron content: A new conception to track solar activity, *Ann. Geophys.*, 26, 335–344.

Balan, N., G. J. Bailey, and B. Jayachandran (1993), Ionospheric evidence for a nonlinear relationship between the solar e.u.v. and 10.7 cm fluxes during an intense solar cycle, *Planet. Space Sci.*, 41(2), 141–145, doi:10.1016/0032-0633(93)90043-2.

Balan, N., G. J. Bailey, B. Jenkins, P. B. Rao, and R. J. Moffett (1994), Variations of ionospheric ionization and related solar fluxes during an intense solar cycle, *J. Geophys. Res.*, 99(A2), 2243–2253, doi:10.1029/93JA02099.

Belehaki, A., G. Moraitis, and I. Tsagouri (2001), The normal state of the F2 ionospheric layer at high latitudes, *Phys. Chem. Earth*, 26(5), 309–313.

Bilitza, D. (2000), The importance of EUV indices for the International Reference Ionosphere, *Phys. Chem. Earth*, 25(5–6), 515–521.

Bilitza, D. (2001), International Reference Ionosphere 2000, *Radio Sci.*, 36, 261–275, doi:10.1029/2000RS002432.

Burešová, D., and J. Laštovička (2000), Hysteresis of foF2 at European middle latitudes, *Ann. Geophys.*, 18, 987–991, doi:10.1007/s00585-000-0987-9.

Chakraborty, S. K., and R. Hajra (2008), Solar control of ambient ionization of the ionosphere near the crest of the equatorial anomaly in the Indian zone, *Ann. Geophys.*, 26, 47–57.

Chen, Y., L. Liu, and H. Le (2008), Solar activity variations of nighttime ionospheric peak electron density, *J. Geophys. Res.*, 113, A11306, doi:10.1029/2008JA013114.

Chen, Y., L. Liu, W. Wan, X. Yue, and S.-Y. Su (2009), Solar activity dependence of the topside ionosphere at low latitudes, *J. Geophys. Res.*, 114, A08306, doi:10.1029/2008JA013957.

Gorney, D. J. (1990), Solar cycle effects on the near-earth space environment, *Rev. Geophys.*, 28(3), 315–336, doi:10.1029/RG028i003p00315.

Guo, J., W. Wan, J. M. Forbes, E. Sutton, R. S. Nerem, T. N. Woods, S. Bruinsma, and L. Liu (2007), Effects of solar variability on thermosphere density from CHAMP accelerometer data, *J. Geophys. Res.*, 112, A10308, doi:10.1029/2007JA012409.

Gupta, J. K., and L. Singh (2001), Long term ionospheric electron content variations over Delhi, *Ann. Geophys.*, 18, 1635–1644, doi:10.1007/s00585-001-1635-8.

Hedin, A. (1984), Correlations between thermospheric density and temperature, solar EUV flux, and 10.7-cm flux variations, *J. Geophys. Res.*, 89(A11), 9828–9834, doi:10.1029/JA089iA11p09828.

Hinteregger, H. E., K. Fukui, and B. R. Gilson (1981), Observational, reference and model data on solar EUV, from measurements on AE-E, *Geophys. Res. Lett.*, 8(11), 1147–1150, doi:10.1029/GL008i011p01147.

Holt, J. M., S.-R. Zhang, and M. J. Buonsanto (2002), Regional and local ionospheric models based on Millstone Hill incoherent scatter radar data, *Geophys. Res. Lett.*, 29(8), 1207, doi:10.1029/2002GL014678.

Huang, C.-M. (1967), On the solar cycle variation of ionospheric F2 layer, *Chin. J. Physiol.*, 5(2), 68–85.

Huang, Y., and K. Cheng (1995), Solar cycle variation of the total electron content around equatorial anomaly crest region in east Asia, *J. Atmos. Terr. Phys.*, 57(12), 1503–1511, doi:10.1016/0021-9169(94)00147-G.

Iijima, B. A., I. L. Harris, C. M. Ho, U. J. Lindqwister, A. J. Mannucci, X. Pi, M. J. Reyes, L. C. Sparks, and B. D. Wilson (1999), Automated daily process for global ionospheric total electron content maps and satellite ocean altimeter ionospheric calibration based on Global Positioning System data, *J. Atmos. Sol. Terr. Phys.*, 61, 1205–1218, doi:10.1016/S1364-6826(99)00067-X.

Judge, D., et al. (1998), First solar EUV irradiances obtained from SOHO by the SEM, *Sol. Phys.*, 177, 161–173, doi:10.1023/A:1004929011427.

Kane, R. P. (1992), Sunspots, solar radio noise, solar EUV and ionospheric foF2, *J. Atmos. Terr. Phys.*, 54(3–4), 463–466, doi:10.1016/0021-9169(92)90025-G.

Kane, R. P. (2003), Solar EUV and ionospheric parameters: A brief assessment, *Adv. Space Res.*, 32(9), 1713–1718, doi:10.1016/S0273-1177(03)90467-4.

Kouris, S. S., P. A. Bradley, and P. Dominici (1998), Solar-cycle variation of the daily foF2 and M(3000)F2, *Ann. Geophys.*, 16, 1039–1042.

Kutiev, I. S., P. G. Marinov, and S. Watanabe (2006), Model of topside ionosphere scale height based on topside sounder data, *Adv. Space Res.*, 37, 943–950, doi:10.1016/j.asr.2005.11.021.

Laštovička, J. (2009), Global pattern of trends in the upper atmosphere and ionosphere: Recent progress, *J. Atmos. Sol. Terr. Phys.*, 71(14–15), 1514–1528.

Lean, J. L., O. R. White, W. C. Livingston, and J. M. Picone (2001), Variability of a composite chromospheric irradiance index during the 11-year activity cycle and over longer time periods, *J. Geophys. Res.*, 106(A6), 10,645–10,658, doi:10.1029/2000JA000340.

Lei, J., L. Liu, W. Wan, and S.-R. Zhang (2005), Variations of electron density based on long-term incoherent scatter radar and ionosonde measurements over Millstone Hill, *Radio Sci.*, 40, RS2008, doi:10.1029/2004RS003106.

Liu, H., H. Lühr, V. Henize, and W. Köhler (2005), Global distribution of the thermospheric total mass density derived from CHAMP, *J. Geophys. Res.*, 110, A04301, doi:10.1029/2004JA010741.

Liu, H., C. Stolle, M. Föster, and S. Watanabe (2007), Solar activity dependence of the electron density in the equatorial anomaly regions observed by CHAMP, *J. Geophys. Res.*, 112, A11311, doi:10.1029/2007JA012616.

Liu, J. Y., Y. I. Chen, and J. S. Lin (2003), Statistical investigation of the saturation effect in the ionospheric foF2 versus sunspot, solar radio noise, and solar EUV radiation, *J. Geophys. Res.*, 108(A2), 1067, doi:10.1029/2001JA007543.

Liu, L., W. Wan, and B. Ning (2004a), Statistical modeling of ionospheric foF2 over Wuhan, *Radio Sci.*, 39, RS2013, doi:10.1029/2003RS003005.

Liu, L., X. Luan, W. Wan, J. Lei, and B. Ning (2004b), Solar activity variations of equivalent winds derived from global ionosonde data, *J. Geophys. Res.*, 109, A12305, doi:10.1029/2004JA010574.

Liu, L., W. Wan, B. Ning, O. M. Pirog, and V. I. Kurkin (2006), Solar activity variations of the ionospheric peak electron density, *J. Geophys. Res.*, 111, A08304, doi:10.1029/2006JA011598.

Liu, L., H. Le, W. Wan, M. P. Sulzer, J. Lei, and M.-L. Zhang (2007a), An analysis of the scale heights in the lower topside ionosphere based on the Arecibo incoherent scatter radar measurements, *J. Geophys. Res.*, 112, A06307, doi:10.1029/2007JA012250.

Liu, L., W. Wan, X. Yue, B. Zhao, B. Ning, and M.-L. Zhang (2007b), The dependence of plasma density in the topside ionosphere on solar activity level, *Ann. Geophys.*, 25(6), 1337–1343.

Liu, L., W. Wan, B. Ning, and M.-L. Zhang (2009), Climatology of the mean TEC derived from GPS Global Ionospheric Maps, *J. Geophys. Res.*, 114, A06308, doi:10.1029/2009JA014244.

Mannucci, A. J., B. D. Wilson, D. N. Yuan, C. M. Ho, U. J. Lindqwister, and T. F. Runge (1998), A global mapping technique for GPS derived ionospheric total electron content measurements, *Radio Sci.*, *33*, 565–582, doi:10.1029/97RS02707.

Mikhailov, A. V., and V. V. Mikhailov (1995), Solar cycle variations of annual mean noon foF2, *Adv. Space Res.*, *15*(2), 79–82, doi:10.1016/S0273-1177(99)80026-X.

Min, K., J. Park, H. Kim, V. Kim, H. Kil, J. Lee, S. Rentz, H. Luhr, and L. Paxton (2009), The 27-day modulation of the low latitudeionosphere during a solar maximum, *J. Geophys. Res.*, *114*, A04317, doi:10.1029/2008JA013881.

Pancheva, D., and P. Mukhtarov (1998), A single-station spectral model of the monthly median foF2 and M(3000)F2, *Stud. Geophys. Geod.*, *42*, 183–196, doi:10.1023/A:1023361105552.

Pandey, V. K., N. K. Sethi, and K. K. Mahajan (2003), Dependence of F2- peak height on solar activity: A study with incoherent scatter measurements, *Adv. Space Res.*, *31*(3), 543–548, doi:10.1016/S0273-1177(03)00049-8.

Rao, M. S. J. G., and R. S. Rao (1969), The hysteresis variation in F2-layer parameters, *J. Atmos. Terr. Phys.*, *31*, 1119–1125, doi:10.1016/0021-9169(69)90110-X.

Rastogi, R. G., and R. P. Sharma (1971), Ionospheric electron content at Ahmedabad (near the crest of equatorial anomaly) by using beacon satellite transmissions during half a solar cycle, *Planet. Space Sci.*, *19*(11), 1505–1517, doi:10.1016/0032-0633(71)90010-9.

Rich, F. J., P. J. Sultan, and W. J. Burke (2003), The 27-day variations of the plasma densities and temperatures in the topside ionosphere, *J. Geophys. Res.*, *108*(A7), 1297, doi:10.1029/2002JA009731.

Richards, P. G. (2001), Seasonal and solar cycle variations of the ionospheric peak electron density: Comparison of measurement and models, *J. Geophys. Res.*, *106*(A7), 12,803–12,819, doi:10.1029/2000JA000365.

Richards, P. G., J. A. Fennelly, and D. G. Torr (1994), EUVAC: A solar EUV flux model for aeronomic calculations, *J. Geophys. Res.*, *99*(A5), 8981–8992, doi:10.1029/94JA00518.

Rishbeth, H. (1993), Day-to-day ionospheric variations in a period of high solar activity, *J. Atmos. Terr. Phys.*, *55*(2), 165–171, doi:10.1016/0021-9169(93)90121-E.

Sethi, N. K., M. K. Goel, and K. K. Mahajan (2002), Solar cycle variations of foF2 from IGY to 1990, *Ann. Geophys.*, *20*, 1677–1685.

Sojka, J. J., C. Smithtro, and R. W. Schunk (2006), Recent developments in ionosphere–thermosphere modeling with an emphasis on solar-variability, *Adv. Space Res.*, *37*(2), 369–379, doi:10.1016/j.asr.2005.10.032.

Su, Y. Z., G. J. Bailey, and S. Fukao (1999), Altitude dependences in the solar activity variations of the ionospheric electron density, *J. Geophys. Res.*, *104*(A7), 14,879–14,891, doi:10.1029/1999JA900093.

Tobiska, W. K., T. Woods, F. Eparvier, R. Viereck, L. Floyd, D. Bouwer, G. Rottman, and O. R. White (2000), The Solar2000 empirical solar irradiance model and forecast toll, *J. Atmos. Sol. Terr. Phys.*, *62*, 1233–1250, doi:10.1016/S1364-6826(00)00070-5.

Trísková, L., and J. Chum (1996), Hysteresis in dependence of foF2 on solar indices, *Adv. Space Res.*, *18*(6), 145–148, doi:10.1016/0273-1177(95)00915-9.

Whalen, J. A. (2004), Linear dependence of the postsunset equatorial anomaly electron density on solar flux and its relation to the maximum prereversal $\mathbf{E} \times \mathbf{B}$ drift velocity through its dependence on solar flux, *J. Geophys. Res.*, *109*, A07309, doi:10.1029/2004JA010528.

Zhang, S.-R., and J. M. Holt (2007), Ionospheric climatology and variability from long-term and multiple incoherent scatter radar observations: Climatology in eastern American sector, *J. Geophys. Res.*, *112*, A06328, doi:10.1029/2006JA012206.

Zhao, B., W. Wan, L. Liu, X. Yue, and S. Venkatraman (2005), Statistical characteristics of the total ion density in the topside ionosphere during the period 1996–2004 using empirical orthogonal function (EOF) analysis, *Ann. Geophys.*, *23*(12), 3615–3631.

———————————

Y. Chen and L. Liu, Beijing National Observatory of Space Environment, Institute of Geology and Geophysics, Chinese Academy of Sciences, Beijing 100029, China. (liul@mail.iggcas.ac.cn)